Journal Pre-proof

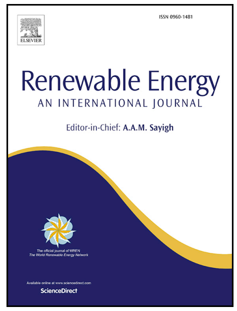

Evaluating the suitability of Sentinel-1 SAR data for offshore wind resource assessment around Cyprus

Stylianos Hadjipetrou, Stelios Liodakis, Anastasia Sykioti, Loukas Katikas, No-Wook Park, Soteris Kalogirou, Evangelos Akylas, Phaedon Kyriakidis

PII: S0960-1481(21)01566-4

DOI: https://doi.org/10.1016/j.renene.2021.10.100

Reference: RENE 16169

To appear in: *Renewable Energy*

Received Date: 13 December 2020

Revised Date: 29 October 2021

Accepted Date: 31 October 2021

Please cite this article as: Hadjipetrou S, Liodakis S, Sykioti A, Katikas L, Park N-W, Kalogirou S, Akylas E, Kyriakidis P, Evaluating the suitability of Sentinel-1 SAR data for offshore wind resource assessment around Cyprus, *Renewable Energy* (2021), doi: https://doi.org/10.1016/j.renene.2021.10.100.

Stylianos Hadjipetrou: Conceptualization, Data curation, Formal analysis, Funding acquisition, Investigation, Methodology, Software, Validation, Visualization, Writing - original draft, Writing - review and editing. **Stelios Liodakis:** Conceptualization, Data curation, Formal analysis, Funding acquisition, Methodology, Software, Validation, Visualization, Writing - original draft, Writing - review and editing. **Anastasia Sykioti:** Data curation, Formal analysis, Funding acquisition, Software, Validation. **Loukas Katikas:** Data curation, Validation. **No-Wook Park:** Conceptualization, Funding acquisition, Investigation, Methodology, Software, Validation. **Soteris Kalogirou:** Validation, Editing. **Evangelos Akylas:** Conceptualization, Investigation, Resources, Validation. **Phaedon Kyriakidis:** Conceptualization, Funding acquisition, Investigation, Methodology, Review and Editing, Project administration, Resources, Supervision.

Evaluating the Suitability of Sentinel-1 SAR data for Offshore Wind Resource Assessment around Cyprus

Hadjipetrou Stylianos*[a,c], Liodakis Stelios[a], Sykioti Anastasia[a], Katikas Loukas[d], Park No-Wook[e], Kalogirou Soteris[b], Akylas Evangelos[a,c], Kyriakidis Phaedon[a,c]

[a] Department of Civil Engineering and Geomatics, Cyprus University of Technology, Limassol 3036, Cyprus (sk.hadjipetrou@edu.cut.ac.cy, stelios.liodakis@cut.ac.cy, anastasia.sykioti@cut.ac.cy, evangelos.akylas@cut.ac.cy, phaedon.kyriakidis@cut.ac.cy)
[b] Department of Mechanical Engineering and Materials Science and Engineering, Cyprus University of Technology, Limassol 3036, Cyprus (soteris.kalogirou@cut.ac.cy)
[c] Eratosthenes Centre of Excellence, Limassol 3036, Cyprus
[d] Department of Topography, Cartography Laboratory, School of Rural and Surveying Engineering, National and Technical University of Athens, Athens 15780, Greece (loukaskatikas@gmail.com)
[e] Department of Geoinformatic Engineering, Inha University, Incheon 22212, Korea (nwpark@inha.ac.kr)

*Corresponding Author
Email: sk.hadjipetrou@edu.cut.ac.cy
Address: Achilleos 1 Bldg., 1st Floor, 2-8 Saripolou Str., 3036 Lemesos, Cyprus
Telephone: +35799897205

Evaluating the suitability of Sentinel-1 SAR data for offshore wind resource assessment around Cyprus

Abstract

Offshore wind offers an excellent opportunity for domestic renewable energy production with a vast potential for future energy systems. Offshore wind resource assessment, however, can be challenging. Remote sensing data e.g., Synthetic Aperture Radar (SAR), provide high spatial resolution detailed information on the spatial variability of offshore wind and have been used for wind resource assessment, as well as for the long-term validation of wind speed estimates from other sources (e.g. Numerical Weather Prediction models). This paper focuses on the evaluation of a 26-month time-series of Sentinel-1 SAR Level 2 OCN products for wind resource assessment in the offshore areas around Cyprus. Sentinel data were evaluated against a 10-year regional reanalysis dataset (UERRA) time-series and wind measurements from 5 coastal meteorological stations in Cyprus. Comparison revealed an overall agreement between the fitted stations and Sentinel Weibull distributions while discrepancies exist between the two data sources and UERRA. Bias observed between Sentinel and UERRA Weibull-derived statistics appears to be spatially dependent. Preliminary wind power assessment results indicate a significant wind power potential for the southwestern offshore areas of Cyprus, surpassing 400 W/m^2 on average, offering thus economically viable solutions in terms of a future offshore wind power project development.

Keywords: Sentinel-1, Coastal meteorological stations, UERRA, Validation, Weibull.

1 Introduction

Renewable Energy Sources (RES), and especially wind energy, have been under the spotlight more than ever, as climate change effects are becoming more evident and severe. The growing climate emergency signifies an unprecedented momentum for the disengagement of the energy market from the unsustainable fossil fuel-based energy production. Recent studies show that wind will be the key to facing the above challenges and drive the markets away from carbon energy [1,2]. While onshore wind technology has already reached a mature stage, offshore wind is still emerging as an attractive source of energy due to the high wind power potential that characterizes the sea. Latest figures indicate an increasing trend of annual offshore wind installation while the cumulative offshore wind capacity has already surpassed 25 GW [3]. Only in 2019, Europe has added 3.6 GW of net offshore capacity reaching 22 GW in total [4]. This is translated to hundreds of new offshore wind turbines being connected to the grid, while also highlighting the importance of offshore wind technologies for facing island-related energy issues. Cyprus, however, lags this global trend. Despite having the biggest increase in energy demand among the EU-28 since 1990, Cyprus still relies on fossil fuels imports to meet the increasing energy demands. As a consequence, Cyprus has not yet achieved the targets set by the EU regarding the use of renewable energy sources for energy consumption and the recently developed National Renewable Energy Action Plan. Due to the limited efforts made towards the assessment of its wind potential, only 13% of the total renewable energy in Cyprus is being generated from wind [5], while all of the existing wind farms have been exclusively located onshore. Further efforts should be undertaken to evaluate the country's offshore wind potential which might comprise an opportunity for domestic renewable energy production.

At a global level, several studies have been conducted up to date at various scales for assessing offshore wind resource potential taking advantage of readily available satellite data. In this context, a detailed knowledge of the spatio-temporal variations of the distribution of offshore wind is needed. This information is subsequently used from planners and decision makers for a plethora of applications ranging from wind farm sitting to spatial planning. Synthetic Aperture Radars (SAR) and scatterometers are typically exploited to retrieve the spatial distribution of wind fields along the sea surface while examples where data from both sources are fused to yield more accurate results also exist [6,7]. Although a continuous global-scale time-series of more than 20 years of wind vectors has been developed by scatterometers, providing observations twice per day, these suffer from relatively poor spatial resolution. Another drawback of scatterometers stems from the inconsistency between data derived from different instruments [8]. NSCAT onboard ADEOS-I satellite [9], SeaWinds onboard QuikSCAT and ADEOS-II satellites [10–13], Oceansat-2/OSCAT [14], ASCAT onboard METOP-A/B satellites [15,16] and HY-2A SCAT [17,18] are some of the most widely exploited scatterometers with their spatial resolution ranging between ~12.5-50 km. SAR on the other hand, provide detailed information at a higher spatial resolution, typically around 1 km or lower. Numerous SAR sensors, such as ERS-1/2 [19–21], ENVISAT ASAR [22–24] and later TerraSAR-X [25,26] RADARSAT-1/2 [27–29] and Sentinel-1A/B [30,31], have provided the means for obtaining wind vectors over the ocean surface.

Wind speed, however, is not directly measured by sensors but rather retrieved via the backscattered Normalized Radar Cross Section (NRCS) of the sea surface by utilizing a geophysical model function (GMF). In particular, CMOD functions (e.g. CMOD5, CMOD7) are typically used to retrieve the wind speed from C-band SAR images. [32–34]. Moreover, SAR provide only temporally dispersed snapshots of the wind patterns at certain atmospheric conditions [35]. Therefore, SAR wind field estimates are typically compared and/or validated against in-situ measurements, such as coastal weather monitoring stations and/or buoys, or in the case of the absence of such means, with mesoscale modeling products.

Sentinel-1A/B data have been extensively used in the literature for revealing wind features that are otherwise unable to be identified, especially near the coastlines where the use of coarser resolution images (e.g. Numerical Weather Predictions) hinders the sensing operation of small-scale changes, such as the fluctuations of atmospheric conditions or surface roughness [36]. Some recent case studies include a wind energy potential analysis on the Mediterranean islands using Sentinel-1 satellite data [37] and the validation of Sentinel-1-derived wind speed against in-situ measurements around Ireland [30]. None of the previous studies carried out so far, however, has focused on the area of Cyprus on research regarding the offshore wind resource potential assessment, while only a few are related to the wind over the Mediterranean Sea. Therefore, such an endeavor will provide an added value and benefit for economic, social and technological development at the national level while laying the groundwork for the undertaking of offshore wind farm installation projects. Prior to utilizing Sentinel-1 data towards that purpose, they have to be validated against data sources characterized by longer time-series such as in-situ wind measurements from meteorological stations or widely available regional reanalysis datasets.

In light of the above, this study is focused on a two-stage evaluation process. The first stage involves a statistical comparison of Sentinel-1A & 1B SAR Level 1 wind field estimates against in-situ measurements from five meteorological stations located around Cyprus coast as well as the corresponding regional reanalysis model outputs derived from a 10-year time-series. The second stage pertains to the spatio-temporal comparison between the Sentinel-1 data and UERRA regional reanalysis data over the entire area of interest. An initial estimate of the average wind power density around Cyprus along with the associated uncertainty derived via bootstrap and a preliminary assessment of the potential development and economic viability of a wind power application before being evaluated at a local scale have also been conducted.

2 Data and Initial Processing

2.1 Sentinel-1 Wave Mode SAR Level-2 OCN Products

Sentinel-1 is a SAR constellation of the EU's Copernicus Earth Observation program consisting of two polar orbiting satellites, Sentinel-1A & 1B, launched on 3 April 2014 and 25 April 2016, respectively. Each satellite has a near-polar, sun-synchronous orbit with a 12-day repeat cycle and 175 orbits per cycle while both are sharing the same orbital plane and operating in the C-band 24 hours daily collecting imagery. Since the two satellites share the same orbit with a 180^o orbital phasing difference, the repeat cycle is reduced to 6 days. The high spatial resolution of Sentinel-1 C-band SAR instruments provide detailed information on the spatial variability of offshore wind; hence it can be used for offshore wind resource assessment as well as for the long-term validation of wind speed measurements from various sources. The spatial resolution of Sentinel-1 data can vary depending on the acquisition mode and the level of data processing [38].

In this work, Ocean Wind Fields (OWI) geophysical component data are used from 503 Sentinel-1 Level-2 Ocean (OCN) products with a spatial resolution of 1km and a time frame from May 21, 2017 until July 30, 2019 to match the corresponding time-series of the regional reanalysis dataset used. These refer to ground range gridded estimates of the surface wind speed and direction at the 10m height above the sea surface derived from Sentinel-1 Level-1 Ground Range Detected (GRD) images of Interferometric Wide (IW) Swath mode under Vertical-Vertical (VV) + Vertical Horizontal (VH) dual polarisation operation. Both Sentinel 1A and 1B satellites are recording tiles in the broader offshore Cyprus area approximately at 3:45 Coordinated Universal Time (UTC) and 15:45 UTC, leading to a (spatially partial) coverage of 1 to 2 scenes per day within a 4-day run, leaving 3 days in between without a scene.

The tiles used along with the location of the five coastal weather monitoring stations are depicted with red outline in Figure 1. Tiles tilting to the right occur when both satellites are descending while tiles tilting to the left occur when the satellites are ascending. The tilting of Sentinel products and the spatial micro-variability related to satellite images specify different pseudo-grids almost for each tile. In order to bring all the information at a common basis, all values from the tile pixels were resampled to a regular square grid by assigning Sentinel's pixel values to the closest grid node. A maximum distance of 1 pixel (~1km) was set for the resampling process to prevent long distance allocation of Sentinel-1 pixel values to the regular grid. The regular grid bounding box is shown with white outline in Figure 1.

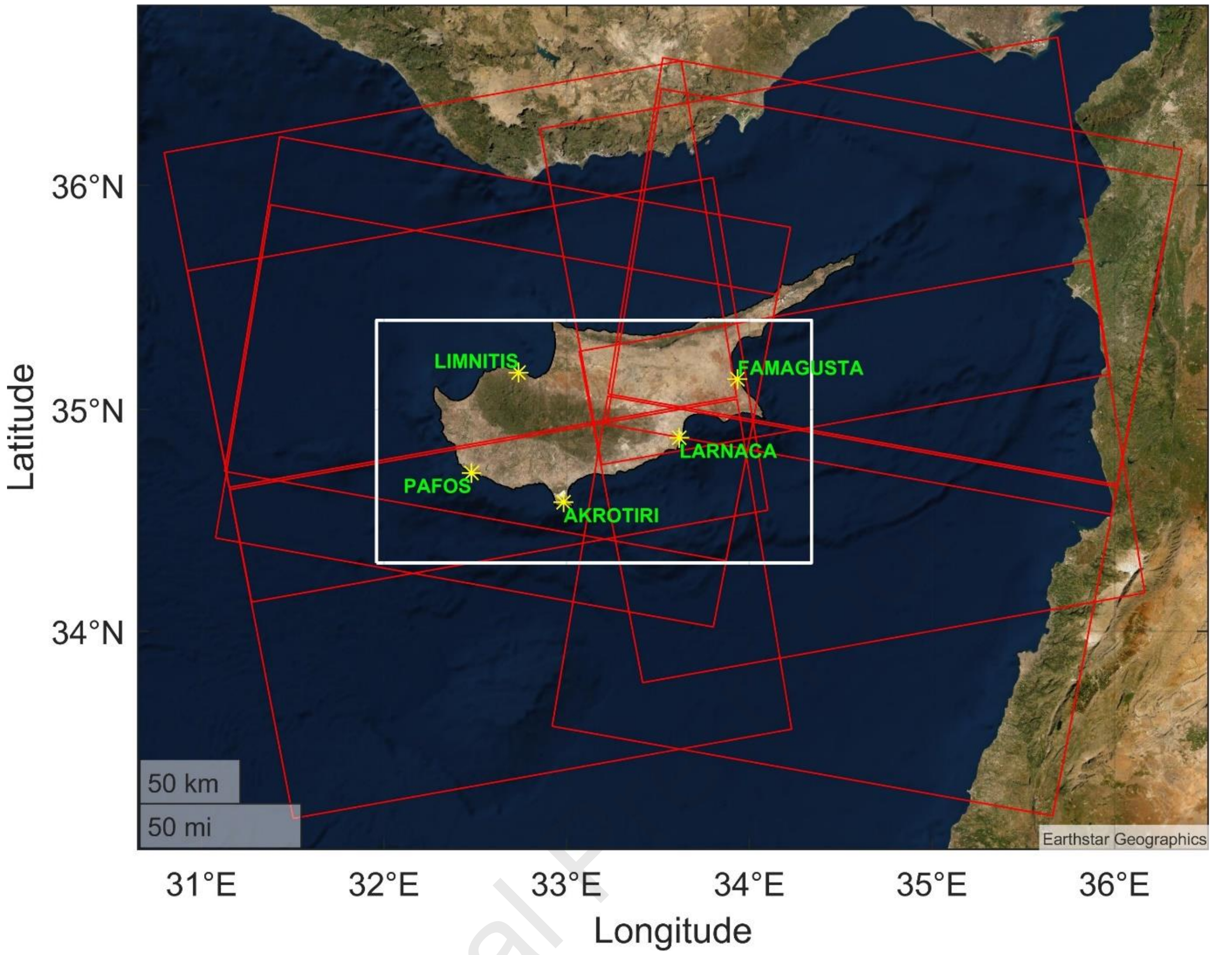

Figure 1: Outline of the study area (white polygon), typical Sentinel tiles within a month's period (red polygons) and weather monitoring stations

All tiles partially overlap in space, resulting in different number of values for each node of the resampled grid. Data at nodes with less than 120 values as well as nodes within a 1.5 km distance from Cyprus's coastline were discarded as SAR backscattering close to the coastal areas may be affected by several parameters, such as bathymetry and surface roughness, increasing the uncertainty of wind speed estimation on these areas [39]. The flag value is related to the inversion quality as well as the geophysical and the NRCS quality estimated. Here, all the SAR wind quality flag values of 3 were completely discarded from each image. Sentinel-1 SAR images also exhibit systematic border noise, resulting in artefacts like 0 or extremely low wind speed values at pixels lying along the east and west image edges [40]. To address this issue, the problematic image rows/columns were completely removed from these images. The resulting number of values at each node after the image preprocessing, is shown in Figure 2. Nodes with many values (~475), depicted in yellow, lie close to Larnaca, while nodes with fewer values (~250) lie close to Limnitis, Pafos and Akrotiri.

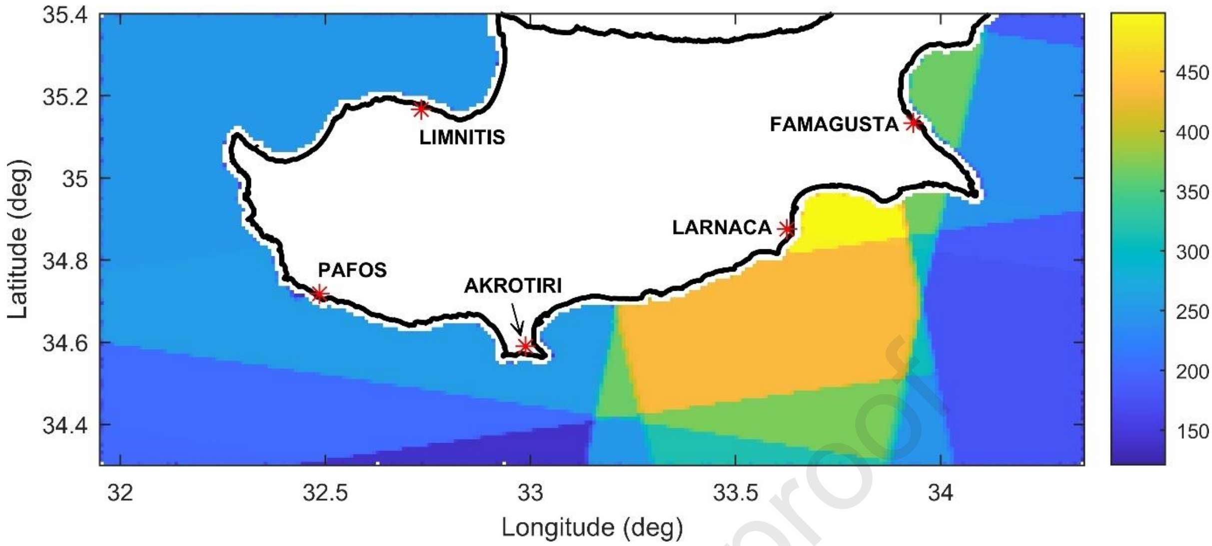

Figure 2: Number of Sentinel values at each node

2.2 Uncertainties in Ensembles of Regional Reanalyses (UERRA)

UERRA regional reanalysis gridded data available by the European Centre for Medium-Range Weather Forecasts (ECMWF) is being used along the lines of this project. UERRA is a dataset derived using a 3-dimensional variational data assimilation system covering the area of Europe and combining meteorological in-situ data with modelled data in order sift good-quality data. The data are available from 1961 onwards. The laws of physics allow for estimates at locations where data coverage is low. The provision of estimates at each grid point in Europe for each regular output time, over a long period, always using the same format, makes reanalysis a very convenient and popular dataset to work with. The dataset's horizontal resolution is 11km and the temporal resolution is 6 hours, starting at 00:00UTC. It provides wind speed and direction at 10m along with several other variables (e.g. relative humidity, temperature, albedo) [41]. UERRA HARMONIE/V1 model outputs, available at the spatial resolution of 11km and at a 6-hour interval, were acquired for the period of January 2009 to July 2019. UERRA data were resampled to a separate regular square grid using the nearest neighbor resampling technique. Although the UERRA cell size grid is different (11km) than the corresponding Sentinel grid, the bounding box was preserved to allow for fair comparisons between the two datasets (Figure 5). UERRA grid data were masked to limit the information included only in the offshore area of Cyprus and a separate cutoff was set for the number of Sentinel-1 nodes contained in each UERRA cell. Therefore, UERRA cells containing less than 80 Sentinel-1 nodes were not considered.

2.3 Data from Cyprus Coastal Meteorological Stations

In-situ wind speed observations from five Cyprus coastal meteorological stations located at Limnitis, Famagusta, Pafos, Akrotiri, and Larnaca areas, as shown in Figure 1, were retrieved online from the NCEI GIS Map Portal available at: https://gis.ncdc.noaa.gov/maps/ncei/cdo/hourly. The database consists of global hourly and synoptic observations obtained from more than 20,000 stations worldwide. The weather information is also accompanied by the reporting format, in accordance with the international code forms. Weather information broadcasted from Cyprus meteorological stations is mainly reported in two formats, namely METAR and SYNOP. The former is a code name for an aerodrome routine meteorological report while the latter refers to surface observations coming from a fixed land station, either manned or automatic. The reporting formats are coded as FM-15 and FM-12, respectively. To form a consistent wind time-series, only the weather information from METAR reports was used where both were available. Therefore, a 10-year time-series of in-situ measurements was formed between January 1, 2009-July 31, 2019 to match the corresponding UERRA time-series. Similar to the SAR data, information related to the data quality was also taken into account during the initial processing of the coastal monitoring station data. Only the data that passed all quality control checks (Q = 1) were used in this study, while data with missing values were discarded. The coordinates and elevation information of each of these stations is included in Table 1. In contrast to SAR data, meteorological stations provide direct wind speed measurements at an hourly basis and thus can be used for Sentinel data validation. The selected stations are also located at a very short distance from the coast and at a relatively flat terrain, allowing thus the comparison between the two sources of wind speed values without considering orographic effects.

Table 1: Coordinates and elevation of the five coastal meteorological stations used for data validation

	Latitude	Longitude	Elevation (m)*
Limnitis	35.1664	32.7369	30
Famagusta	35.1364	33.9356	10
Pafos	34.7154	32.4791	22
Akrotiri	34.5833	32.9833	33
Larnaca	34.8736	33.6173	12

*Elevation refers to Above Mean Sea Level (AMSL) including the mast height (10m)

Vertical extrapolation is applied to the in-situ measurements prior to the comparison in order to bring wind speed values at the Sentinel and UERRA data height (10m above the sea surface). The most common techniques used for the vertical extrapolation of wind speed are the power and logarithmic laws. The former is known to perform better for unstable conditions while the latter is preferred when atmospheric conditions are neutral [42], as assumed here. Given the altitude of the stations as reference height, the extrapolated SAR wind speed at the stations height can be calculated as [43]:

$$u_{(z_r)} = \frac{\ln(\frac{z_r}{z_0})}{\ln(\frac{z}{z_0})} u_{(z)} \quad (1)$$

where $u_{(z_r)}$ the wind speed at the reference height (m/sec), $u_{(z)}$ is the wind speed at height z (m/sec) and z_0 is the surface roughness, which was set to 0.0002 m according to the surface roughness length values given in [44]. Therefore, in-situ measurements were compared to the corresponding values of the closest nodes of Sentinel-1 SAR Level 2 OCN wind speed gridded data to calculate mismatch statistics.

3 Wind Resource Assessment

Following a per-pixel analysis, empirical distribution functions are typically fitted to the data time-series to derive the power density output. The statistical distributions of sample wind speed values over time are mostly positively skewed and are usually modeled using a theoretical Weibull probability distribution function (PDF); other distribution models, e.g., Gamma, have also been used. The Weibull probability density function has been widely used to fit wind speed distributions for wind energy applications as it appears to be related to the nature of the wind in certain conditions [45,46]. The theoretical PDF is fitted to the sample wind speed data by estimating the parameters (scale (α) and shape (β) parameters of the Weibull distribution), so that some measure of agreement between the model-derived and the sample statistics (or quantiles and/or probabilities) is maximized.

Parameter estimation procedures include least-squares, method of moments, maximum likelihood, and variations thereof; in this study, the maximum likelihood method was adopted. Goodness-of-fit statistical tests can also be used (albeit with caution) for deciding on the adoption of alternative PDF models. Moreover, as the statistical distribution of wind speeds varies from place to place around the globe, depending upon local climate conditions, the landscape, and its surface, the Weibull distribution may vary as well, both in its shape, and in its scale value.

3.1 Weibull Distribution Fitting

Weibull distribution probabilities are obtained from:

$$f(x) = \left(\frac{\alpha}{\beta}\right)\left(\frac{x}{\beta}\right)^{\alpha-1} \exp\left[-\left(\frac{x}{\beta}\right)^{\alpha}\right], \quad x, \alpha, \beta > 0. \tag{2}$$

For different values of α, the response of the shape of the distribution changes. When α equals 3.6, for example, the Weibull is very similar to the Gaussian distribution while for shape parameters greater than this, the Weibull density exhibits negative skewness.

208 The mean of the Weibull distribution can be obtained from α and β parameters by:

$$a[\Gamma(1+\beta^{-1})] \quad (3)$$

and the variance by:

$$a^2[\Gamma(1+2\beta^{-1})-\Gamma(1+\beta^{-1})^2] \quad (4)$$

209 where Γ( ) is the Gamma function.

210 Weibull distributions fitted to the data obtained at the five Cyprus coastal meteorological stations are
211 depicted in Figure 3:

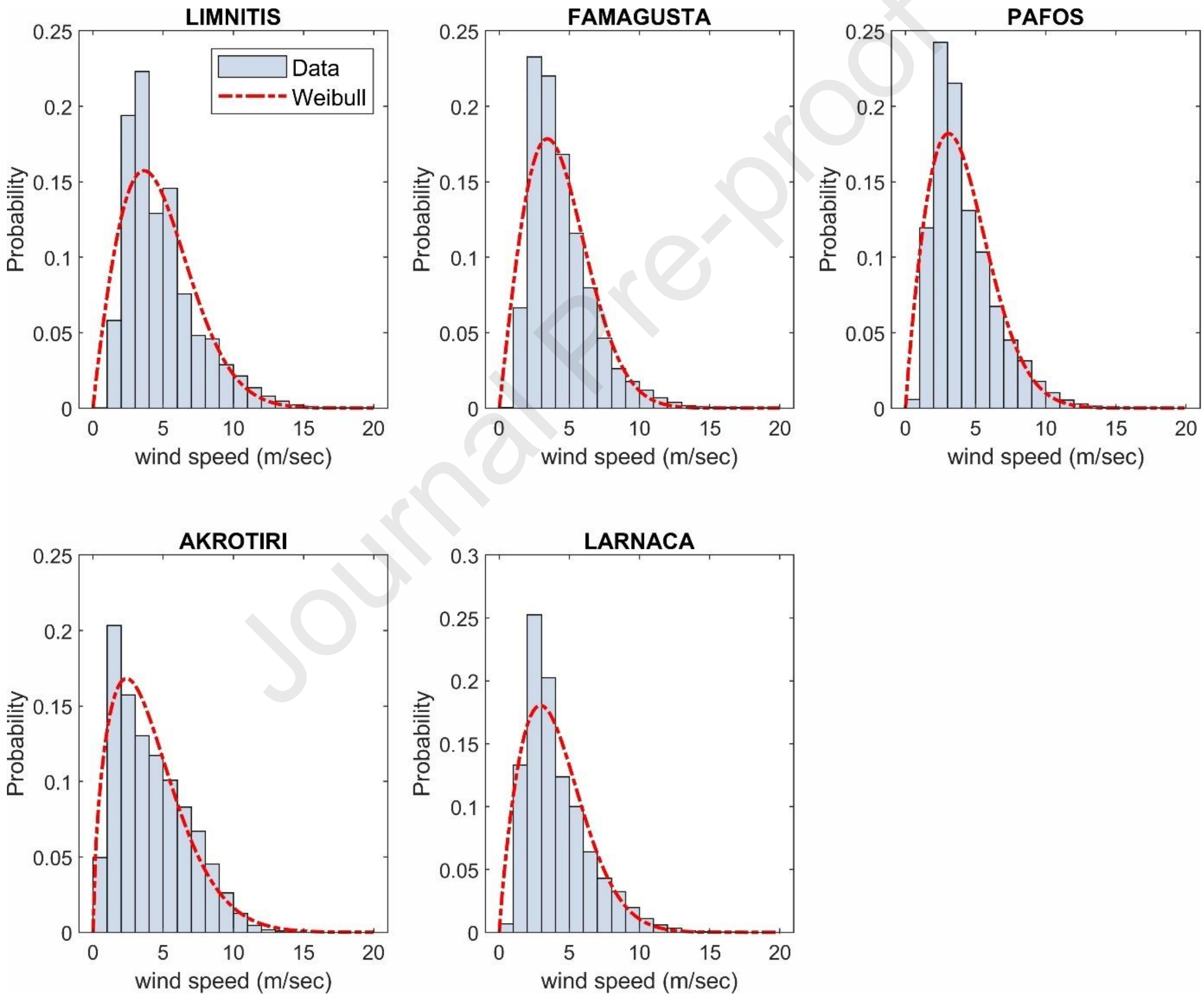

212 *Figure 3: Fitted Weibull distributions to stations data*

213 Weibull distribution fitting was conducted via the method of maximum likelihood using the complete
214 datasets over the 10-year period of interest. An overall agreement is obvious between the empirical
215 histogram and the fitted Weibull distribution at each station location.

3.2 First Stage Statistical Comparison and Evaluation

Shape and scale Weibull parameters derived from the fitted distributions of in-situ measurements were initially compared to the corresponding values of the closest UERRA node along with the Sentinel-1 values spatially lying within the UERRA pixel. The location of the closest UERRA to each station along with the corresponding Sentinel-1 nodes is shown in the following figure:

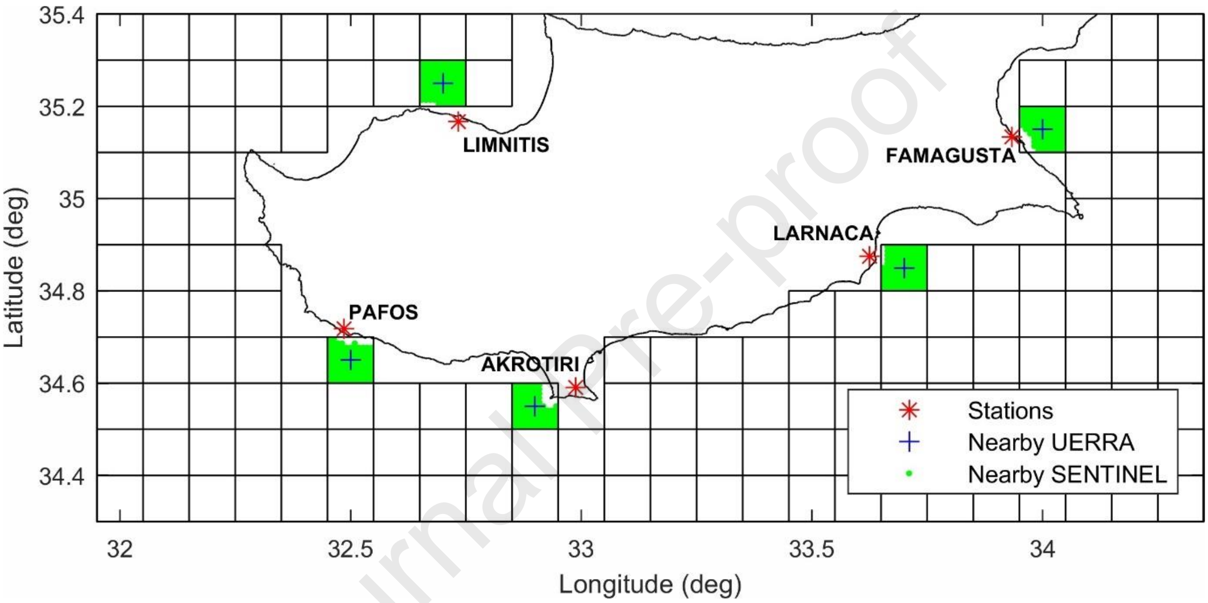

Figure 4: Closest UERRA and corresponding Sentinel nodes to stations

To evaluate the Sentinel-1 data against the in-situ measurements and the UERRA wind speed values, Weibull-derived scale and shape parameters from satellite data were upscaled (by averaging) within each UERRA cell after the fitting. As depicted in Figure 2, the initial Sentinel-1 data processing resulted in different number of nodes within each UERRA cell with the lowest number of Sentinel nodes being 99 within the UERRA cell near Akrotiri station and the highest 117 within the closest UERRA cell to Limnitis station. The fitted Cumulative Distributions Functions (CDFs) of the in-situ data and both the UERRA and Sentinel-1 values from the closest node are shown in Figure 5 for comparison. The staircase appearance of the stations CDFs is due to the rounding of the raw data downloaded from NOAA, most probably due to conversion from the knots to m/sec. A visual review of the figures indicates a good fit of the Weibull distribution as CDFs are quite identical among the three data sources. Minor discrepancies exist between the CDFs of the three data sources, allowing to conclude that there is an overall agreement between the cumulative distributions of in-situ, UERRA and satellite-derived data, apart from the Limnitis area where both the data and Weibull-derived CDFs of UERRA are quite distant from the corresponding distributions of stations and Sentinel-1 data. Furthermore, the errors between the CDFs do not depend on wind speed intensity, as different degrees of errors exist for certain wind speed values when comparing between the locations of interest, although low values seem to correlate particularly well between data at most of the locations.

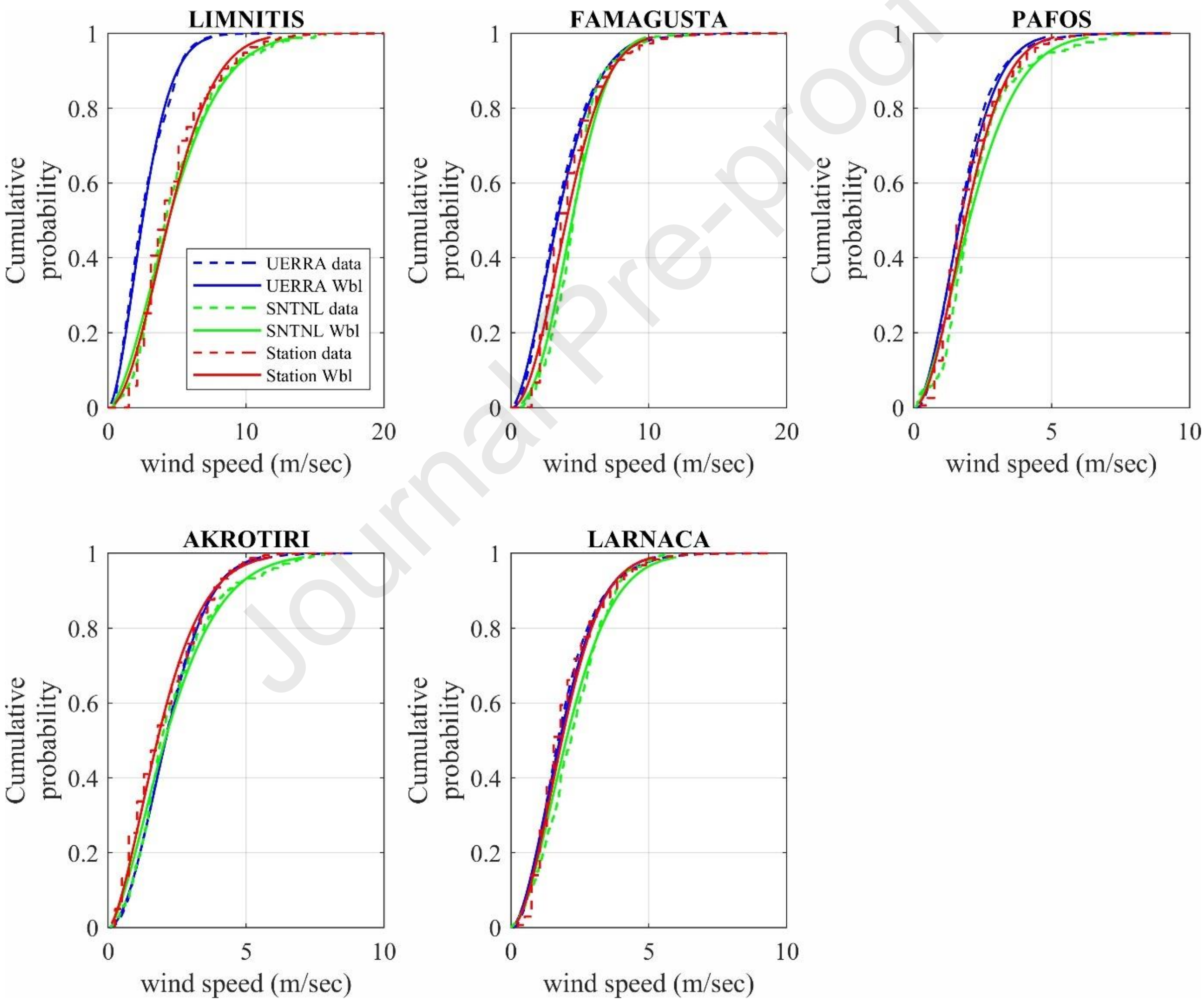

Figure 5: Fitted Weibull CDFs for station data and Sentinel values from nearest node

Moreover, comparing the data with the fitted Weibull CDFs, allows to conclude that the Weibull fitting did not alter the relative relationship between UERRA, stations and Sentinel data in general even that some degree of bias has been introduced as anticipated. We can, therefore, use the Weibull-fitted data to assess the wind speed and estimate the wind power density, as demonstrated in the final section.

The fitted distributions parameters as well as the Weibull-derived mean and standard deviation of the three data sources are summarized in Table 2. A slight overestimation of Sentinel-1 scale parameter over the other two data sources in all the locations is evident while the shape parameter appears to be location dependent. Overall, the upscaled Sentinel Weibull parameters and statistics are higher correlated with their station counterparts rather than the ones derived from the UERRA fitted Weibull distributions. This is more obvious, when comparing the mean and standard deviation among all the available data sources. Both the mean and the standard deviation derived from the UERRA fitted Weibull distribution appear to be quite low in most of the cases comparing to the ones extracted from stations and upscaled Sentinel distributions.

Table 2: Fitted Weibull parameters and statistics for stations data, closest UERRA node and upscaled Sentinel values from the closest UERRA node

	Station				Upscaled Sentinel				UERRA			
	Scale (α)	Shape (β)	Mean	Std dev	Scale (α)	Shape (β)	Mean	Std dev	Scale (α)	Shape (β)	Mean	Std dev
Limnitis	5.32	1.92	4.72	2.55	5.47	1.67	4.89	3.01	3.15	1.75	2.75	1.65
Famagusta	4.82	2.01	4.27	2.21	5.16	2.39	4.58	2.05	4.26	1.73	3.72	2.26
Pafos	4.55	1.89	4.04	2.22	5.03	1.67	4.50	2.80	4.21	1.85	3.67	2.09
Akrotiri	4.50	1.58	4.04	2.62	5.24	1.53	4.72	3.14	5.14	1.97	4.47	2.41
Larnaca	4.51	1.84	4.00	2.26	4.98	1.78	4.44	2.60	4.45	1.77	3.89	2.30

A visual comparison between the Weibull-derived statistics from the three data sources at the areas close to each meteorological station and prior to upscaling the Sentinel parameters is depicted in Figure 6. As already stated above, a slight overestimation of the stations statistics by the Sentinel exists while UERRA Weibull-derived statistics, on the contrary, seem to slightly underestimate the in-situ measurements. UERRA mean exhibits the higher discrepancy from the other two data sources, especially close to Limnitis meteorological station where the difference between the Weibull-derived mean values is higher than 2 m/sec. Overall, it can be said that stations and Sentinel Weibull-derived statistics tend to agree quite well at most of the locations. UERRA parameters, on the other hand, appear unstable throughout the locations of interest as they tend to underestimate the parameters of the rest data sources except at the area of Akrotiri.

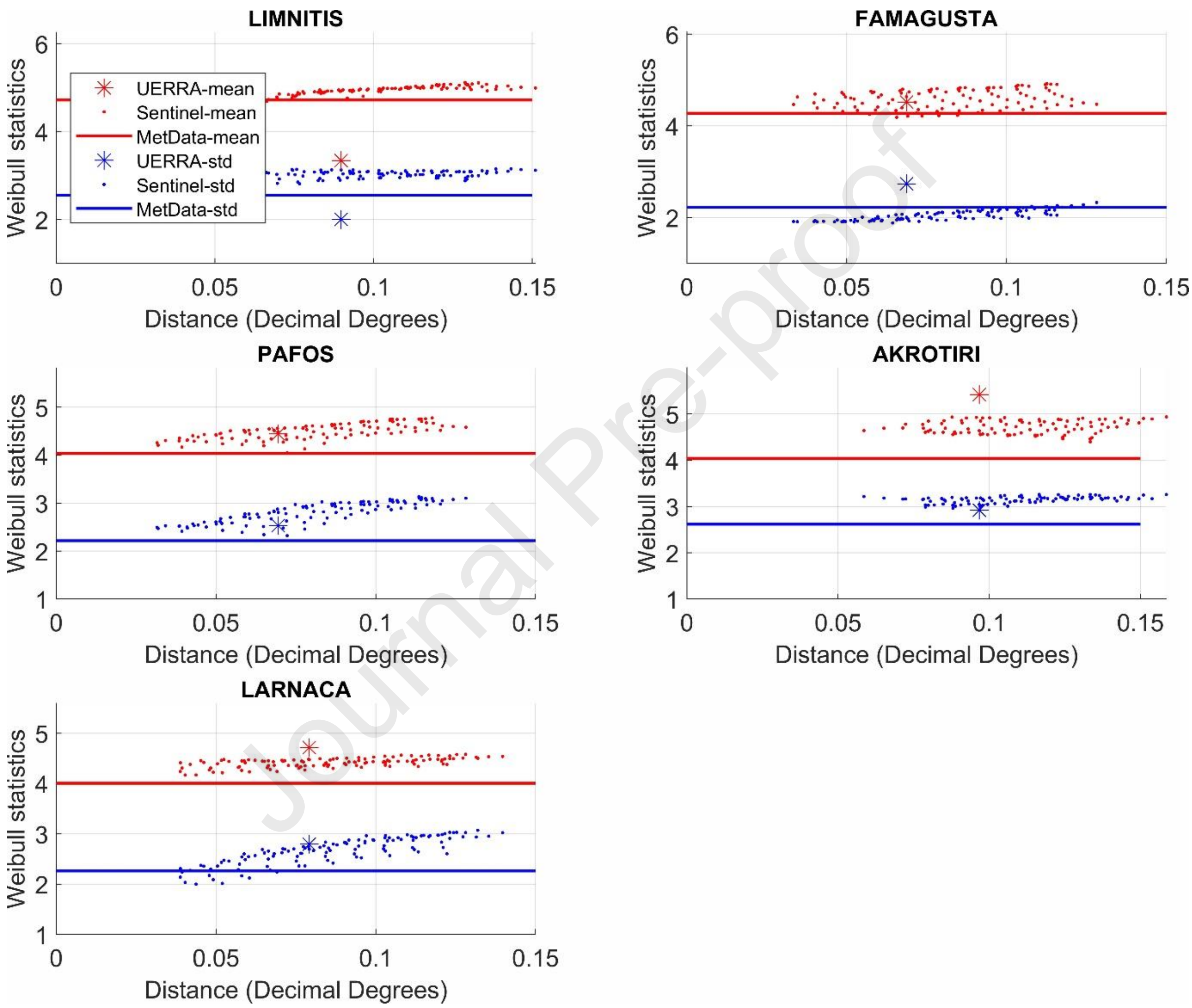

Figure 6: Comparison between UERRA, stations and Sentinel-1 Weibull-derived statistics (mean and standard deviation)

3.3 Second Stage Statistical Comparison and Evaluation

In this section, we investigate the comparison between the UERRA and Sentinel with regards to the reproduction of their corresponding Weibull distributions statistics. Prior to the comparison, Sentinel Weibull parameters were upscaled (by averaging) at the level of UERRA grid size; meaning that the average value of Weibull statistics were calculated for the Sentinel nodes located in each UERRA cell. The two data sources were initially compared in terms of the reproduction of the Weibull-derived mean and standard deviation. Areas colored in yellow correspond to higher UERRA values comparing to the Sentinel while the opposite is true for all the color shades of green and blue. The two maps of Figure 7 differ in terms of orientation of the spatial patterns of the difference between the Sentinel and UERRA Weibull-derived mean and standard deviation. In the first case (difference between the mean) a slight overestimation of the Sentinel is obvious at the areas below ~35 degrees of latitude while Sentinel mean is underestimated by the UERRA in the northern areas and especially close to Limnitis meteorological station; in accordance with the first CDF of Limnitis of Figure 5.

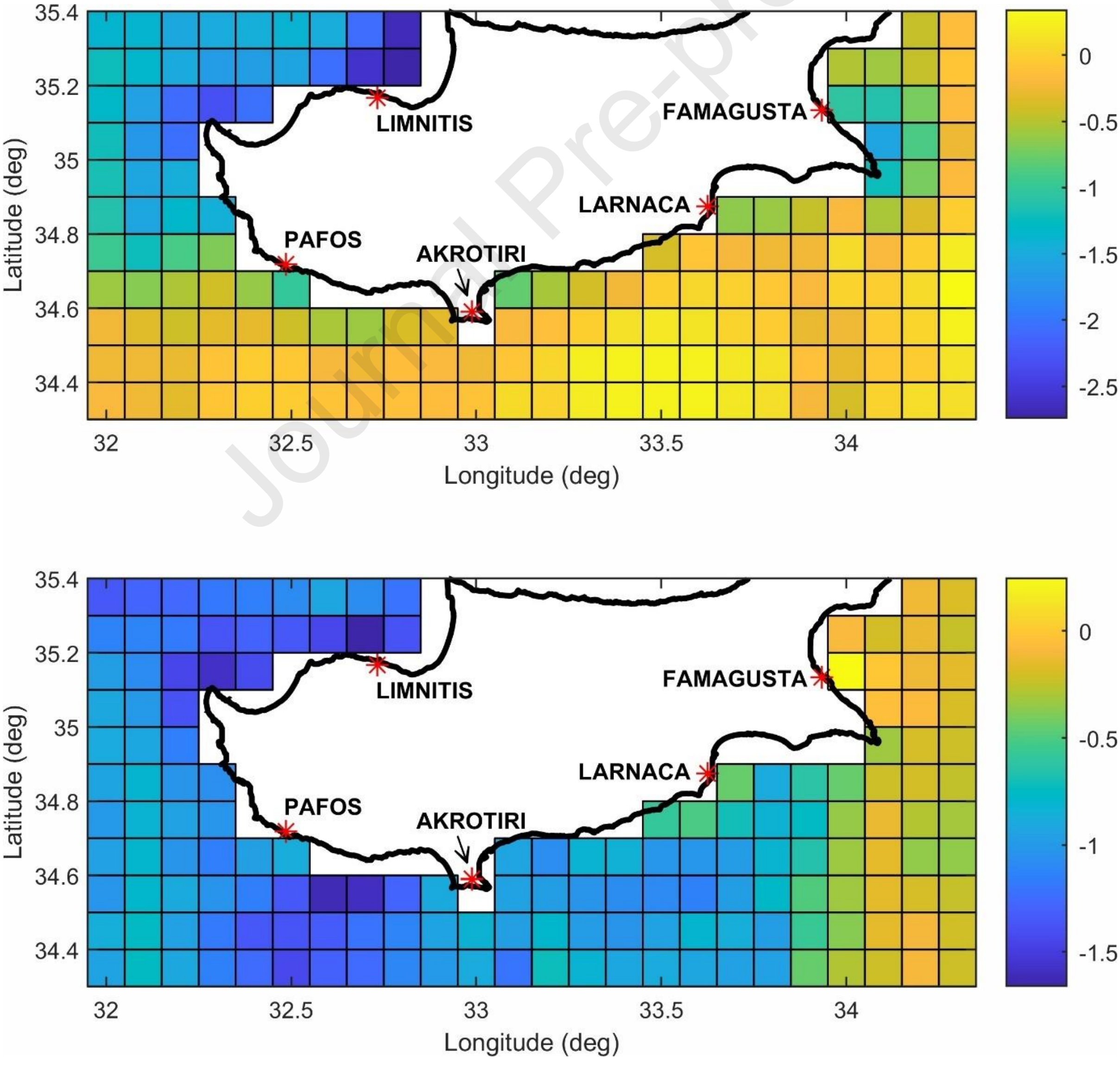

Figure 7: Difference between UERRA and Sentinel Weibull-derived mean (top), and standard deviation (bottom)

A vertical separation is evident in the second case where the Weibull-derived standard deviation of the two data sources is compared. In this case, Sentinel standard deviation proves to be higher in most of the UERRA cells. This underestimation is spatially clustered around the eastern areas, especially after 34 degrees of longitude. It should be also noted that values in areas close to the coast are clearly affected by several parameters e.g., the number of Sentinel nodes, the sensor sensitivity and land orographic effects. Overall, Sentinel presents higher standard deviation values allowing to conclude that the range of its' wind speed distribution is generally wider compared to UERRA. With the above being said, one could argue that the two data sources provide a complementary aspect in reproducing the wind speed distributions along with the associated statistics and parameters.

4 Preliminary Wind Power Potential Assessment

The average wind power density P in (W/m^2), is the average kinetic energy passing through a unit of surface per unit of time and represents a key quantity in wind resource assessment studies. When wind speed time series are available, P can be estimated directly from the data as:

$$P_{(s)} = 0.5\rho \frac{1}{N}\sum_{i=1}^{N} s_i^3 \tag{5}$$

where ρ is the air density (1.225 kg/m^3 at 15°C) and s_i is the wind speed value.

Being proportional to the cube of wind speed [47], wind-derived energy has been proved to follow Weibull distribution, typically described by scale and shape When a Weibull distribution is fitted to sample data, the average wind power density is expressed in terms of the Weibull PDF parameters (α and β) as:

$$P_w = 0.5\rho a^3 \Gamma\left(1 + \frac{3}{b}\right) \tag{6}$$

This is a shortcut to the estimation of wind power density via integration as:

$$P_w = 0.5\rho \int s^3 f\ (s; a, b)\, ds \tag{7}$$

As the typical offshore wind turbine hub height is close to 100m, wind speed values from in-situ and satellite data were extrapolated to the above-mentioned height using equation (1) in order to estimate average wind power. Therefore, as of this point, the 100m will be the reference height for wind energy as presented in the rest of this section. Wind power density was subsequently calculated by applying equation (4) after Weibull distribution was fitted to each pixel's time-series. Sentinel-1 SAR Level-2 OCN data were primarily used to calculate wind power for offshore areas of Cyprus. As several studies have demonstrated [48–51], the offshore area around Cyprus is characterized on average by low intensity wind flows. More precisely, the power density for 5686 SAR nodes ranges between 200-250 W/m^2 while 7917 nodes between 275-325 W/m^2. The lowest wind power density value was found to be 94 W/m^2, located at the northwest gulf of Cyprus approximately 0.25 decimal degrees west from Limnitis station while the highest (420 W/m^2) lies 0.2 decimal degrees south of Akrotiri station. Figure 8 shows the average wind power density calculated over the 26-month period of interest.

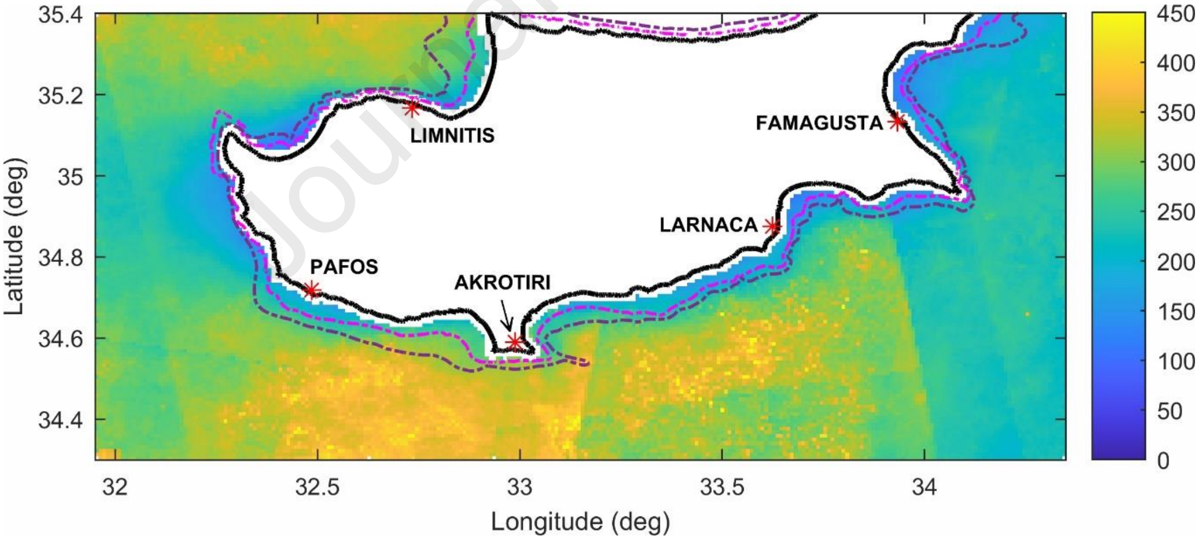

Figure 8: Sentinel average (Weibull-derived) wind power density (W/m^2) over the 26-month period of interest. Isodepth contour lines of 100 and 300 meters are shown with magenta and purple colors, respectively.

As wind power is mathematically proportional to the cube of wind speed, similar patterns of high and low wind speed values are expected. In particular, low wind power density values appear on average very close to the coast while the highest values (>400 W/m^2) are clustered at the south and north offshore parts of Cyprus, as well as some small patches east of Famagusta station. Especially the southwestern area, which combines the high wind power density with the relatively short distance to the coast, seems to offer a significant potential and an opportunity for both a power productive and economically viable solution in terms of a wind power application. Unfortunately, due to the different number of Sentinel samples at each grid cell (Fig. 2) some sharp edges also exist in the images leading to less reliable Weibull fits and therefore non-realistic wind power density patterns. A clear general picture of the satellite-derived wind power density patterns along the year in the offshore area of Cyprus can be shaped. Moreover, the reliability of the Sentinel-1 sample wind speed values will be increasing in parallel with the increase in the number of satellites passes over the area of interest. Nevertheless, Cyprus's steep bathymetry gradient, as depicted in Figure 8, implies that any offshore wind farm installation endeavor would be economically viable at relatively small distances from the coast, even in the case of floating wind turbines.

A bootstrap method was also employed to further examine the uncertainty related to the wind power density assessment as shown in Figure 9.

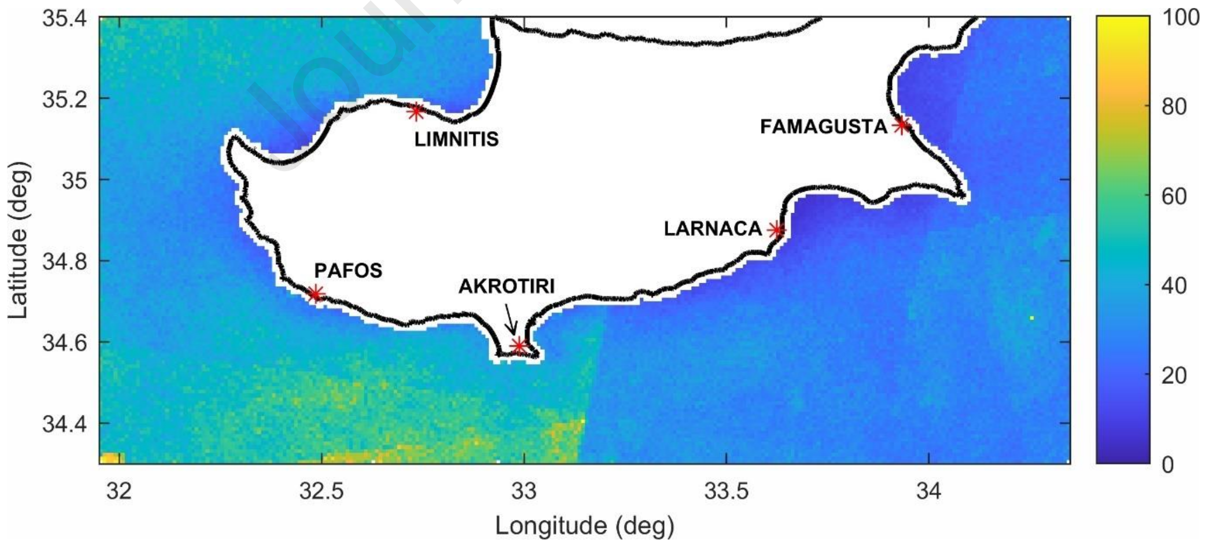

Figure 9: Standard deviation of the bootstrap resampled (Weibull-derived) wind power density (W/m^2) over the 26-month period of interest

The standard deviation obtained via a set of 100 bootstrap samples of Sentinel wind speed data associated with each node. This resulted in a set of 100 fitted Weibull distributions and a histogram of the same number of wind power density values at each node. By juxtaposing the maps from Figure 8 and 9, one can clearly see that higher wind power density values are associated with higher uncertainty even though these areas do not necessarily correspond to a higher number of Sentinel nodes. Sharp edges, however, due to the difference between the number of nodes still exist.

4.1 Wind Power Density Seasonal Analysis and Comparison

The main seasonal properties of satellite-derived wind power density compared to the corresponding of UERRA were also investigated in this study over the 26-month period. In this study, the seasons are considered as follows: Winter (December-January-February (DJF)), Spring (March-April-May (MAM)), Summer (June-July-August (JJA)) and Fall (September-October-November (SON)). Figure 10 shows the average Sentintel-1 SAR Level 2 OCN Weibull-derived wind power density per season for the period of interest.

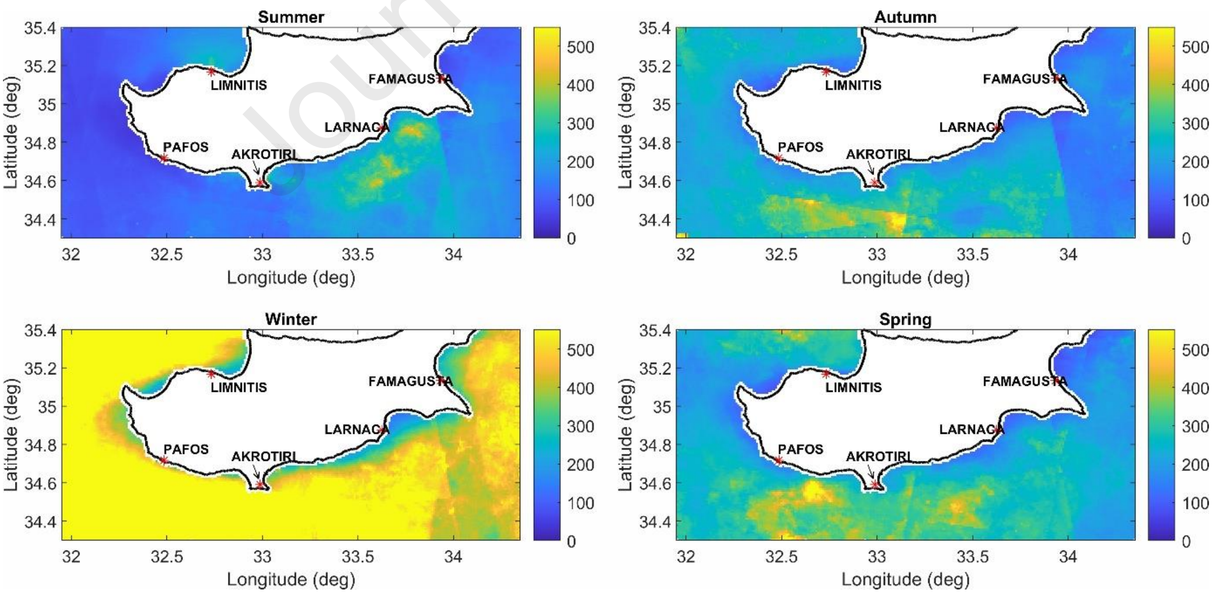

Figure 10: Average Sentinel Weibull-derived wind power density (W/m^2) per season over the 26-month period of interest

The seasonal average Sentinel Weibull-derived wind power density patterns (Figure 10) confirm what was expected regarding the wind trends. Low intensity winds producing a wind power density of 139

(W/m^2) on average and strong winds surpassing a wind power density of 300 (W/m^2) on average have been estimated over the area of interest and the 26-month period for the summer and winter seasons, respectively. It should be stressed however that the particularly high wind power density values in Winter, depicted in Figure 10, are highly affected by a number of Sentinel images (~10 time instances spread over winter) where the wind speed values are estimated to be extremely high (between 15-25 m/sec) throughout the whole area of study. Including these images in the average wind power density calculation, results in an average additional ~200 (W/m^2), mainly clustered in the central eastern and western offshore parts around Cyprus. High wind power density patterns of winter seem to hold until spring although power density is being gradually weakened. Autumn is associated with moderate winds which account for 225 (W/m^2) on average. Both Summer and Autumn seasons do not seem to offer much wind resource potential favoring a wind power application in regard to the location of the higher wind power density patterns. Spring and Winter, on the other hand, offer a significant potential, especially in the areas south of Pafos and Limassol where the seawater depth would allow for an offshore wind farm installation.

Similar spatial patterns are observed when visualizing the Weibull-derived UERRA average wind power density (Figure 11), albeit smoother and at lower scales.

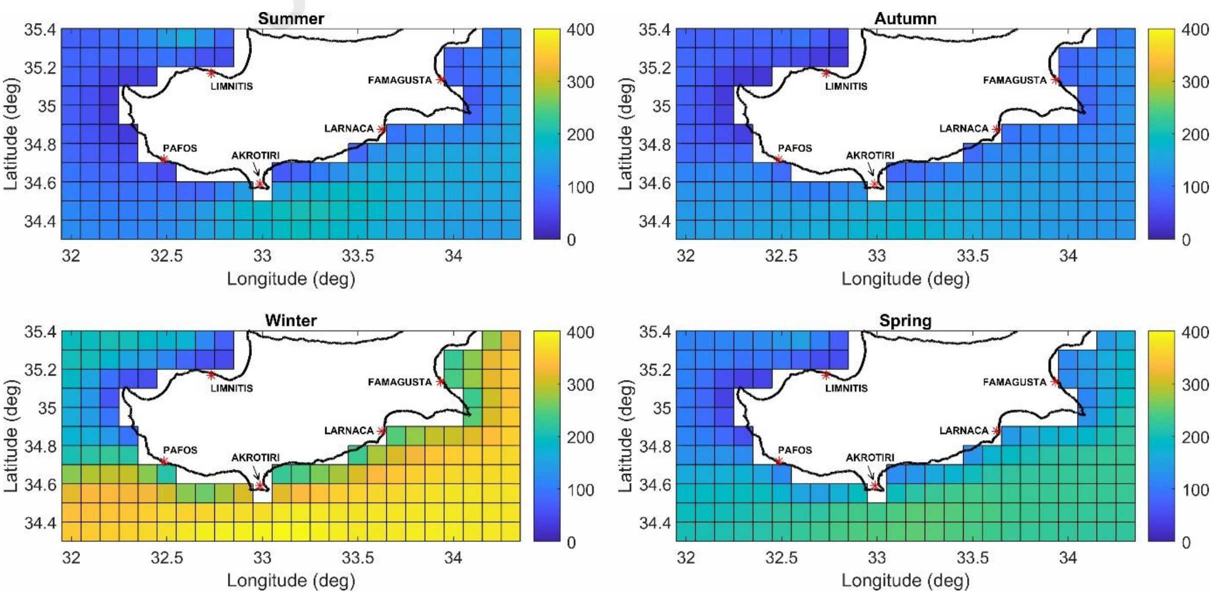

Figure 11: Average UERRA Weibull-derived wind power density (W/m^2) per season over the 26-month period of interest

More specifically, the maximum wind power density values during the winter lie close to 400 W/m^2 while the same value during the rest of the seasons ranges mostly between 150-250 W/m^2.

In general, wind speed values from 3.5 to 6.5 m/sec prevail most of the time around the year, or, more precisely, from March to November. Strong wind flows are coming from the Western and Central Mediterranean region with an eastward direction before they are divided by Cyprus's land mass. Wind speed values are then gradually decreased to ~5-6.5 m/sec. On the other hand, the lowest winds are mapped close to Larnaca and Limnitis meteorological stations where the two bays and the local topography seem to affect the local wind currents. Unfortunately, due to the different number of Sentinel samples at each grid cell some sharp edges also exist in the images leading to less reliable Weibull fits and therefore non-realistic spatial patterns. Nevertheless, a clear general picture of the satellite-derived wind power density patterns along the year in the offshore area of Cyprus can be shaped. Moreover, the reliability of the SAR sample wind speed values will be increasing in parallel with the increase in the number of satellites passes over the area of interest. For the 26-month period under investigation, the highest number of samples per season was 110-115 while the lowest, beside the pixels lying close to the coast, was close to 30. These, however, are located far from the coast where wind farm sitting seems to be non-viable due to the deep bathymetry and the large distance from the coast.

5 Conclusions and Future Work

In this work, Sentinel 1 SAR Level 2 OCN wind field estimates were statistically compared and validated against in-situ measurements from five meteorological stations located along Cyprus coast and UERRA regional reanalysis model outputs. Prior to the comparison, Weibull distributions were fitted to the wind time-series and both the Weibull parameters as well as the main statistics were extracted. The data and fitted CDFs seem match well, allowing to conclude that the initial values were not affected from the fitting. The first stage of the comparison showed an overall agreement between the stations and Sentinel data, while considerable discrepancies exist between the first two data sources and

UERRA. Erroneous values seem to affect the robustness of the analysis and therefore should be treated with caution. The second stage involved the comparison between Sentinel and UERRA Weibull-derived statistics over the complete study area. The deviations expressed in terms of the differences of the means proved to vary spatially, differentiating between the northern and southern parts of the area of interest.

As Sentinel-1 Level 2 OCN products were validated against more accurate in-situ wind speed measurements, the wind speed distribution of these data can also be used to estimate wind power over a particular area of interest. Sentinel wind speed estimates were extrapolated to the wind turbine hub height and Weibull distributions were then fitted to each Sentinel wind speed time-series prior to estimating the wind power. Sentinel-1 SAR Level 2 OCN Weibull-derived average wind power density over the 26-month period of interest showed that particularly high wind power density values are spatially clustered in the south parts of the area of interest. The same areas are characterized by higher uncertainty in the reproduction of wind power density. An assessment of these areas, considering also the seawater depth, implies that an economically viable wind farm installation would be ideally sited close to the offshore areas close to Akrotiri and Pafos meteorological stations. Cyprus' steep bathymetry gradient, however, highlights the need for a more detailed, local scale, assessment. The difference shape between the number of samples due to satellite swath is also obvious in the average wind power density maps estimated from SAR images. As the satellites continue to span Cyprus's offshore area, more samples will be available leading to more reliable wind speed estimates obtained by the Sentinel-1 images. The seasonal analysis output indicated large variations between the different seasons. Particularly high wind power density values were observed during the winter along the North- and Southeast parts of the area of interest, while wind power density during summer and autumn ranges between 150-200 (W/m^2) on average.

The main drawback of Level 2 products is the short time-series which may lead to unreliable wind resource assessments in some instances. Wind retrieval from Sentinel-1 Level 1 products can also be achieved in order to obtain a wider time-series. In particular, the Department of Wind Energy of the Technical University of Denmark has been systematically retrieving wind fields from SAR data (e.g. Sentinel-1, ENVISAT and TerraSAR-X) in order to deliver a freely availably wind archive covering the seas around Europe and other areas. Wind fields retrieved from Sentinel-1 products are available via their online portal at https://satwinds.windenergy.dtu.dk/. Therefore, future work will be focused on the comparison between wind field estimates obtained from Sentinel-1 Level 1 and Level-2 products which can be also validated against in-situ measurements from meteorological stations and/or buoys.

Lastly, taking advantage of the spatial resolution of SAR data, downscaling techniques can be performed in order to spatially enhance the coarse resolution information of wind products provided by regional scale Numerical Weather Prediction (NWP) models, or, viewed alternatively, provide additional temporal information to wind resource assessments based on Sentinel-1 data.

ACKNOWLEDGMENTS

This work is funded by the European Regional Development Fund and the Republic of Cyprus through the Research and Innovation Foundation (Project: INTERNATIONAL/OTHER/0118/0120).

REFERENCES

[1] G.W.E. Council, Global wind report 2018. Global Wind Energy Council: Brussels, Belgium., (2019). https://gwec.net/global-wind-report-2019/ (accessed July 13, 2020).

[2] D. Carvalho, A. Rocha, M. Gómez-Gesteira, C. Silva Santos, Potential impacts of climate change on European wind energy resource under the CMIP5 future climate projections, Renew. Energy. 101 (2017) 29–40. https://doi.org/10.1016/j.renene.2016.08.036.

[3] W. Energy, O. Special, Offshore Wind Outlook 2019: World Energy Outlook Special Report, 2019. www.iea.org/t&c/ (accessed July 13, 2020).

[4] WindEurope, Offshore wind in Europe - Key trends and statistics 2020, 2021. https://windeurope.org/intelligence-platform/product/offshore-wind-in-europe-key-trends-and-statistics-2020/ (accessed August 10, 2021).

[5] N. Kythreotou, Cyprus' Integrated national energy and climate plan for the period 2021-2030, 2020.

[6] C.B. Hasager, A. Mouche, M. Badger, F. Bingöl, I. Karagali, T. Driesenaar, A. Stoffelen, A. Peña, N. Longépé, Offshore wind climatology based on synergetic use of Envisat ASAR, ASCAT and QuikSCAT, Remote Sens. Environ. 156 (2015) 247–263.

https://doi.org/10.1016/j.rse.2014.09.030.

[7] R. Chang, R. Zhu, M. Badger, C. Hasager, X. Xing, Y. Jiang, Offshore Wind Resources Assessment from Multiple Satellite Data and WRF Modeling over South China Sea, Remote Sens. 7 (2015) 467–487. https://doi.org/10.3390/rs70100467.

[8] A. Bentamy, S.A. Grodsky, A. Elyouncha, B. Chapron, F. Desbiolles, Homogenization of scatterometer wind retrievals, Int. J. Climatol. 37 (2017) 870–889. https://doi.org/10.1002/joc.4746.

[9] M.H. Freilich, R.S. Dunbar, The accuracy of the NSCAT 1 vector winds: Comparisons with National Data Buoy Center buoys, J. Geophys. Res. Ocean. 104 (1999) 11231–11246. https://doi.org/10.1029/1998jc900091.

[10] R.F. Sánchez, P. Relvas, H.O. Pires, Comparisons of ocean scatterometer and anemometer winds off the southwestern Iberian Peninsula, Cont. Shelf Res. 27 (2007) 155–175. https://doi.org/10.1016/j.csr.2006.09.007.

[11] M.W. Spencer, Improved resolution backscatter measurements with the SeaWinds pencil-beam scatterometer, IEEE Trans. Geosci. Remote Sens. 38 (2000) 89–104. https://doi.org/10.1109/36.823904.

[12] F. Pimenta, W. Kempton, R. Garvine, Combining meteorological stations and satellite data to evaluate the offshore wind power resource of Southeastern Brazil, Renew. Energy. 33 (2008) 2375–2387. https://doi.org/10.1016/j.renene.2008.01.012.

[13] I. Karagali, A. Peña, M. Badger, C.B. Hasager, Wind characteristics in the North and Baltic Seas from the QuikSCAT satellite, Wind Energy. 17 (2014) 123–140. https://doi.org/10.1002/we.1565.

[14] R. Kumar, A. Chakraborty, A. Parekh, R. Sikhakolli, B.S. Gohil, A.S.K. Kumar, Evaluation of oceansat-2-derived ocean surface winds using observations from global buoys and other scatterometers, IEEE Trans. Geosci. Remote Sens. 51 (2013) 2571–2576. https://doi.org/10.1109/TGRS.2012.2214785.

[15] T. Remmers, F. Cawkwell, C. Desmond, J. Murphy, E. Politi, The potential of advanced scatterometer (ASCAT) 12.5 km coastal observations for offshore wind farm site selection in Irish waters, Energies. 12 (2019). https://doi.org/10.3390/en12020206.

[16] C.C. Lin, W. Lengert, E. Attema, Three Generations of C-Band Wind Scatterometer Systems From ERS-1/2 to MetOp/ASCAT, and MetOp Second Generation, IEEE J. Sel. Top. Appl. Earth Obs. Remote Sens. 10 (2017) 2098–2122. https://doi.org/10.1109/JSTARS.2016.2616166.

[17] D. Li, H. Shen, Evaluation of wind vectors observed by HY-2A scatterometer using ocean buoy observations, ASCAT measurements, and numerical model data, Chinese J. Oceanol. Limnol. 33 (2015) 1191–1200. https://doi.org/10.1007/s00343-015-4136-4.

[18] M. Zheng, X.M. Li, J. Sha, Comparison of sea surface wind field measured by HY-2A scatterometer and WindSat in global oceans, J. Oceanol. Limnol. 37 (2019) 38–46. https://doi.org/10.1007/s00343-019-7347-2.

[19] C.B. Hasager, M. Nielsen, P. Astrup, R. Barthelmie, E. Dellwik, N.O. Jensen, B.H. Jørgensen, S.C. Pryor, O. Rathmann, B.R. Furevik, Offshore wind resource estimation from satellite SAR wind field maps, Wind Energy. 8 (2005) 403–419. https://doi.org/10.1002/we.150.

[20] C.B. Hasager, M. Nielsen, O. Rathmann, B.R. Furevik, T. Hamre, Offshore wind maps from ERS-2 SAR and wind resource modelling, in: Int. Geosci. Remote Sens. Symp., 2003: pp. 2709–

2711. https://doi.org/10.1109/igarss.2003.1294559.

[21] T. Schneiderhan, S. Lehner, J. Schulz-Stellenfleth, J. Horstmann, Comparison of offshore wind park sites using SAR wind measurement techniques, Meteorol. Appl. 12 (2005) 101–110. https://doi.org/10.1017/S1350482705001659.

[22] R. Chang, R. Zhu, M. Badger, C.B. Hasager, R. Zhou, D. Ye, X. Zhang, Applicability of synthetic aperture radar wind retrievals on offshore wind resources assessment in Hangzhou Bay, China, Energies. 7 (2014) 3339–3354. https://doi.org/10.3390/en7053339.

[23] M. Badger, C.B. Hasager, A.P. Diaz, A.N. Hahmann, P. Volker, Wind resources at turbine height from Envisat and Sentinel-1 SAR, (2016).

[24] C.B. Hasager, M. Badger, A. Peña, X.G. Larsén, F. Bingöl, SAR-based wind resource statistics in the Baltic Sea, Remote Sens. 3 (2011) 117–144. https://doi.org/10.3390/rs3010117.

[25] X.-M. Li, S. Lehner, S. Brusch, Y.-Z. Ren, Sea surface wind measurement over offshore wind farm using TerraSAR-X data, in: Remote Sens. Ocean. Sea Ice, Coast. Waters, Large Water Reg. 2011, SPIE, 2011: p. 81750M. https://doi.org/10.1117/12.910331.

[26] X.M. Li, S. Lehner, Observation of terra SAR-X for studies on offshore wind turbine wake in near and far fields, IEEE J. Sel. Top. Appl. Earth Obs. Remote Sens. 6 (2013) 1757–1768. https://doi.org/10.1109/JSTARS.2013.2263577.

[27] P. Beaucage, G. Lafrance, J. Lafrance, J. Choisnard, M. Bernier, Synthetic aperture radar satellite data for offshore wind assessment: A strategic sampling approach, J. Wind Eng. Ind. Aerodyn. 99 (2011) 27–36. https://doi.org/10.1016/j.jweia.2010.10.005.

[28] P.W. Vachon, F.W. Dobson, Wind Retrieval from RADARSAT SAR Images: Selection of a Suitable C-Band HH Polarization Wind Retrieval Model, Can. J. Remote Sens. 26 (2000) 306–313. https://doi.org/10.1080/07038992.2000.10874781.

[29] J. Brainard, A. Lovett, J. Parfitt, Assessing hazardous waste transport risks using a GIS, Int. J. Geogr. Inf. Syst. 10 (1996) 831–849. https://doi.org/10.1080/02693799608902112.

[30] L. de Montera, T. Remmers, C. Desmond, R. O'Connell, Validation of Sentinel-1 offshore winds and average wind power estimation around Ireland, (2019) 1–24. https://doi.org/10.5194/wes-2019-49.

[31] T. Ahsbahs, M. Badger, I. Karagali, X.G. Larsén, Validation of Sentinel-1A SAR Coastal Wind Speeds Against Scanning LiDAR, Remote Sens. 9 (2017) 552. https://doi.org/10.3390/rs9060552.

[32] A. Stoffelen, D. Anderson, Scatterometer data interpretation: Estimation and validation of the transfer function CMOD4, J. Geophys. Res. C Ocean. 102 (1997) 5767–5780. https://doi.org/10.1029/96JC02860.

[33] H. Hersbach, A. Stoffelen, S. De Haan, An improved C-band scatterometer ocean geophysical model function: CMOD5, J. Geophys. Res. Ocean. 112 (2007). https://doi.org/10.1029/2006JC003743.

[34] Y. Lu, B. Zhang, W. Perrie, A.A. Mouche, X. Li, H. Wang, A C-Band geophysical model function for determining coastal wind speed using synthetic aperture radar, IEEE J. Sel. Top. Appl. Earth Obs. Remote Sens. 11 (2018) 2417–2428. https://doi.org/10.1109/JSTARS.2018.2836661.

[35] C.B. Hasager, B.R. Furevik, On offshore wind energy mapping using satellite SAR, Can. J. Remote Sens. 28 (2002) 80–89. https://doi.org/10.5589/m02-008.

[36] X. Yang, X. Li, Q. Zheng, X. Gu, W.G. Pichel, Z. Li, Comparison of ocean-surface winds retrieved from quikscat scatterometer and radarsat-1 SAR in offshore waters of the U.S. West Coast, IEEE Geosci. Remote Sens. Lett. 8 (2011) 163–167. https://doi.org/10.1109/LGRS.2010.2053345.

[37] M. Majidi Nezhad, D. Groppi, P. Marzialetti, L. Fusilli, G. Laneve, F. Cumo, D.A. Garcia, Wind energy potential analysis using Sentinel-1 satellite: A review and a case study on Mediterranean islands, Renew. Sustain. Energy Rev. 109 (2019) 499–513. https://doi.org/10.1016/j.rser.2019.04.059.

[38] P. Vincent, M. Bourbigot, H. Johnsen, P. Riccardo, Sentinel-1 Product Specification, 2020.

[39] F.M. Rana, M. Adamo, R. Lucas, P. Blonda, Sea surface wind retrieval in coastal areas by means of Sentinel-1 and numerical weather prediction model data, Remote Sens. Environ. 225 (2019) 379–391. https://doi.org/10.1016/j.rse.2019.03.019.

[40] I. Ali, S. Cao, V. Naeimi, C. Paulik, W. Wagner, Methods to Remove the Border Noise from Sentinel-1 Synthetic Aperture Radar Data: Implications and Importance for Time-Series Analysis, IEEE J. Sel. Top. Appl. Earth Obs. Remote Sens. 11 (2018) 777–786. https://doi.org/10.1109/JSTARS.2017.2787650.

[41] O.A. Ridal M., Olsson E., Unden P., Zimmermann K., UERRA Deliverable D2.7 HARMONIE reanalysis report of results and dataset., Seventh Framework Programme Theme 6 [SPACE], available at: http://www.uerra.eu/, last access: 6 March 2020., (2017).

[42] C. Xu, C. Hao, L. Li, X. Han, F. Xue, M. Sun, W. Shen, Evaluation of the power-lawwind-speed extrapolation method with atmospheric stability classification methods for flows over different terrain types, Appl. Sci. 8 (2018). https://doi.org/10.3390/app8091429.

[43] J.F. Manwell, J.G. McGowan, A.L. Rogers, Wind Energy Explained: Theory, Design and Application, Wiley, 2010. https://doi.org/10.1002/9781119994367.

[44] H. Charnock, Wind stress on a water surface, Q. J. R. Meteorol. Soc. 81 (1955) 639–640. https://doi.org/10.1002/qj.49708135027.

[45] J.E. Oliver, ed., Encyclopedia of World Climatology, Springer Netherlands, 2005. https://doi.org/10.1007/1-4020-3266-8.

[46] D. Wilks, Statistical Methods in the Atmospheric Sciences, Elsevier, 2019. https://doi.org/10.1016/c2017-0-03921-6.

[47] T. Burton, N. Jenkins, D. Sharpe, E. Bossanyi, Wind Energy Handbook, Second Edition, 2011. https://doi.org/10.1002/9781119992714.

[48] F. Onea, L. Deleanu, L. Rusu, C. Georgescu, Evaluation of the wind energy potential along the Mediterranean Sea coasts, Energy Explor. Exploit. 34 (2016) 766–792. https://doi.org/10.1177/0144598716659592.

[49] D. Pantusa, G.R. Tomasicchio, Large-scale offshore wind production in the Mediterranean Sea, Cogent Eng. 6 (2019). https://doi.org/10.1080/23311916.2019.1661112.

[50] I. Koletsis, V. Kotroni, K. Lagouvardos, T. Soukissian, Assessment of offshore wind speed and power potential over the Mediterranean and the Black Seas under future climate changes, Renew. Sustain. Energy Rev. 60 (2016) 234–245. https://doi.org/10.1016/j.rser.2016.01.080.

[51] T. Soukissian, F. Karathanasi, P. Axaopoulos, Satellite-Based Offshore Wind Resource Assessment in the Mediterranean Sea, IEEE J. Ocean. Eng. 42 (2017) 73–86. https://doi.org/10.1109/JOE.2016.2565018.

Declaration of interests

☒ The authors declare that they have no known competing financial interests or personal relationships that could have appeared to influence the work reported in this paper.

☐The authors declare the following financial interests/personal relationships which may be considered as potential competing interests: